Science of the Total Environment 912 (2024) 169067

Contents lists available at ScienceDirect

Science of the Total Environment

journal homepage: www.elsevier.com/locate/scitotenv

Assessing community health risks from exposure to ultrafine particles containing transition metals in the Greater Houston Area

Wei-Chung Su [a,b,*], Jinho Lee [a], Masoud Afshar [b], Kai Zhang [c], Inkyu Han [d]

[a] Department of Epidemiology, Human Genetics and Environmental Sciences, School of Public Health, University of Texas Health Science Center at Houston, Houston, TX, USA
[b] Southwest Center for Occupational and Environmental Health, School of Public Health, University of Texas Health Science Center at Houston, Houston, TX, USA
[c] Department of Environmental Health Sciences, School of Public Health, University at Albany, State University of New York, Rensselaer, NY, USA
[d] Department of Epidemiology and Biostatistics, College of Public Health, Temple University, Philadelphia, PA, USA

HIGHLIGHTS

- Mobile Aerosol Lung Deposition Apparatus (MALDA) serves as a useful tool to study outdoor ultrafine particle (UFP) exposure.
- By obtaining respiratory deposition and chemical composition of UFPs, health risks posed by urban UFPs can be well assessed.
- No significant transition metal-induced non-cancer and cancer health risks were found via exposure to UFPs in Houston.

GRAPHICAL ABSTRACT

ARTICLE INFO

Editor: Hai Guo

Keywords:
Ultrafine particle
Respiratory deposition
Transition metal
Urban area
Health risk

ABSTRACT

Ultrafine particles (UFPs) in urban air environments have been an essential public health concern. The inhalation of UFPs can introduce transition metals contained in the UFP into the human airways, leading to adverse health effects. Therefore, it is crucial to investigate urban air UFP exposure and health risks induced by transition metals. This research carried out a series of field measurements to study urban air UFP exposure in the Greater Houston Area. Three sampling sites in the Greater Houston Area representing varying levels of UFP exposures were selected. The newly developed Mobile Aerosol Lung Deposition Apparatus (MALDA) which consists of a complete set of human airway replicas and a pair of UFP particle sizers was deployed in the sampling sites during three sampling timeframes (morning rush hours, noon, and afternoon rush hours) to obtain on-site UFP respiratory deposition data. UFP samples were collected at the sampling sites for metal composition analysis. The acquired UFP respiratory deposition data and UFP composition data were then used to calculate the respiratory deposited mass of transition metals and estimate the associated health risks for individuals living near sampling sites. Our results showed that transition metal-induced non-cancer risks caused by exposure to urban UFPs were within acceptable limits. The estimated lifetime excess cancer risks were generally $<10^{-6}$, indicating an overall acceptable level of transition metal-induced cancer risk.

* Corresponding author at: University of Texas Health Science Center at Houston, 1200 Pressler St., Houston, TX 77030, USA.
E-mail address: Wei-Chung.Su@uth.tmc.edu (W.-C. Su).

https://doi.org/10.1016/j.scitotenv.2023.169067
Received 22 September 2023; Received in revised form 6 November 2023; Accepted 1 December 2023
Available online 2 December 2023

1. Introduction

Ultrafine particles (UFPs) are airborne particulate matter with diameters <100 nm. UFPs in urban ambient environments have been, and continue to be an important community health concern. Many thermal processes, such as diesel engine combustion, coal/biomass burning, and photochemical reactions, are known to generate high concentrations of UFPs in urban ambient environments (Moreno-Rıos et al., 2022). UFPs can drift in the air longer than submicron- and micron-size particles due to their nanoscale size. Thus, UFPs are inevitable to be inhaled by people living in urban communities when having outdoor activities. After being inhaled into the human airways, UFPs can easily follow the airstream to penetrate the upper airways, reach the alveolar region in the lower airways, and deposit within it mainly due to the diffusion deposition mechanism. The inhalation and consequent deposition of UFPs in the human airways can lead to detrimental biological responses. For example, exposure to diesel exhaust particles emitted by truck engines can cause lung cancer and cardiovascular dysfunction (Bhatia et al., 1998; Langrish et al., 2013). Inhalation of ultrafine fly ash generated from coal burning processes could cause chronic pulmonary diseases (Chen et al., 1990; Ibald-Mulli et al., 2002). Houston is the fourth largest city in the U.S., with considerable UFPs released from heavy traffic, oil refineries, heavy industries, and the ship channel (Bahreini et al., 2009). Therefore, the communities around the Greater Houston Area are ideal for studying urban UFP exposure and the associated health risks.

Due to the source of generation, UFPs often contain toxic substances such as black carbon (BC), polycyclic aromatic hydrocarbons (PAHs), and metals (Micic et al., 2003; Chen et al., 2005; Wierzbicka et al., 2014; Utsunomiya et al., 2004; Moreno-Rıos et al., 2022). When UFPs are inhaled and deposited in the human pulmonary region, UFPs themselves and the toxic substances carried by UFPs can be translocated into the human circulatory system. The toxic substances can infiltrate cellular-level biological defenses, triggering cascading inflammation processes that lead to detrimental health consequences like pulmonary and systemic inflammation (Moreno-Rıos et al., 2022; Ohlwein et al., 2019). UFPs also have been shown to translocate to the brain via the olfactory nerve after the deposition on the olfactory epithelium located at the roof of the nasal cavity (Oberdörster et al., 2004; Shang et al., 2021).

Among the toxic substance present in UFPs, it is known that transition metals such as cadmium (Cd) and manganese (Mn) can induce reactive oxidative stress (ROS) and systemic inflammation, which can cause cardiorespiratory effects in the human body through a series of physiological mechanisms (Sørensen et al., 2005; Wei et al., 2009; Wittkopp et al., 2013). A positive correlation was reported between the metal concentration in the blood and the metal level in the ambient particulate matter (Gangwar et al., 2019). Transition metals are known to induce other adverse health effects such as lung, brain, liver damage, and even lung cancer (Carter et al., 1997; Donaldson et al., 2000; Donaldson et al., 2001; Schraufnagel, 2020). Table 1 lists the health effects induced by transition metals through the inhalation route. Values of reference dose (*RfD*), cancer slop factors (*CSF*), and carcinogen classification of a specific transition metal are also listed in the table. Among these selected transition metals, hexavalent chromium (Cr VI), nickel (Ni), and cadmium (Cd) can cause both non-cancer and cancer effects. The rest of the metals can cause either non-caner or cancer effects. Hence, it is important to investigate the composition of transition metals in UFPs. With this in mind, the focus of this study was on assessing transition metal-associated health risks arising from exposure to UFPs in urban environments.

When assessing health risks caused by the inhalation of UFPs, acquiring the deposited mass (intake mass) of UFPs in the respiratory system is essential. The deposited mass represents the inhaled UFPs remaining in the airways, which is a crucial factor in estimating inhalation doses for toxic substances contained in UFPs (e.g., transition metals). To obtain an accurate deposited mass of UFPs, it relies on correct UFP respiratory deposition fractions because it is known that not all inhaled UFPs will remain within (deposit) the human airways, contributing to the dosage. A considerable portion of inhaled UFPs could exit out of the respiratory system through the exhaled air without deposition. The UFP respiratory deposition fraction is known as a function of the UFP diameter. UFPs of different sizes will have various deposition fractions in different airway regions. Therefore, by knowing the size distribution of UFPs in typical urban UFP exposure and the proportion of the inhaled UFP deposits in the airways, a more precise UFP respiratory deposited mass can be estimated for urban populations. With further understanding of the composition of transition metals in UFPs, health risks caused by exposure to transition metal-contained urban UFPs can then be well assessed.

To date, although some UFP respiratory deposition studies have been published, most of the studies were carried out in the laboratory. No UFP respiratory deposition experiments to our knowledge were conducted in outdoor environments to study respiratory deposition of urban UFP. The lack of real-life respiratory deposition studies was mainly attributed to the requirement of specialized laboratory apparatus used in the traditional experimental methods (Cheng et al., 1993; Cohen et al., 1990). Moreover, the human airway replicas used in previous respiratory deposition studies were generally limited to the human upper airways due to the technical challenge in the past of making lower airway replicas (Smith et al., 2001; Su and Cheng, 2015). As a result, with UFP respiratory deposition data only available in the upper airways, data acquired was considered not useful in studying associated health risks since UFP-induced respiratory effects are known to be primarily in the

Table 1
Toxic transition metals and the associated health effects through inhalation exposure.

Metal	Non-Cancer Effects*	RfD$ (mg/kg-day)	Cancer Effects* (Carcinogen Classification)	CSF $(mg/kg\text{-}day)^{-1}$
Chromium (Cr VI)	Lactate dehydrogenase in bronchioalveolar lavage fluid	2.9E-05	Lung Cancer (EPA: A; IARC: 1)	42
Manganese (Mn)	Impaired lung and neurobehavioral functions	1.4E-05	–	–
Lead (Pb)	Altered neurosensory function	–	(EPA: B2; IARC: 2B)	0.042
Nickel (Ni)	Lung inflammation	2.6E-05	Lung Cancer (EPA: A; IARC: 1)	0.8
Antimony (Sb)	Pneumoconiosis and laryngitis	8.6E-05	–	–
Vanadium (V)	Lung damage	2.9E-05	–	–
Arsenic (As)	Respiratory irritation	–	Lung Cancer (EPA: A; IARC: 1)	15.1
Cobalt (Co)	Asthma-like allergy and decreased lung function	2.9E-05	(IARC: 2B)	–
Cadmium (Cd)	Emphysema and decreased lung function	2.9E-06	Lung Cancer (EPA: B1; IARC: 1)	6.3
Uranium (U)	Initial body weight loss and moderate nephrotoxicity	5.7E-04	–	–

* Sources of health effects: U.S. Agency for Toxic Substances and Disease Registry (ATSDR) ToxGuide™ and US EPA Integrated Risk Information System (IRIS).
$ RfD was converted by RfC using a reasonable inhalation rate of 20 m^3/day and a default body weight of 70 kg (i.e., RfD = RfC × 20/70).

Table 2
The sampling sites, site characteristics, and sampling season.

Sampling Site	Site Description	Sampling Season
Park Place Blvd. (PP)	• Residential area • The location is close to an 8-lane (I-610 South) (1.6 km) and 10-lane (I-45 South Freeway) (1.6 km) freeway. • The average annual $PM_{2.5}$ in 2018 was 11.7 μg/m^3 (SD: ± 5.9 μg/m^3). • Traffic emissions from I-45 may be the primary contributor to UFPs in this location.	May to Jul. 2021 (Data with 17 sets of MALDA and 1 set of MOUDI)[$]
		Jan. to Mar. 2022 (Data with 22 sets of MALDA and 1 set of MOUDI)
Clinton Dr. (CD)	• Industrial area • Located approximately 800 m from the 10-Lane I-610 East Freeway. This monitoring site is located to the north of the Port of Houston Authority and shipyards along the Houston Ship Channel. The railroad also runs parallel to the Clinton Drive where the monitoring site is located. • The average annual $PM_{2.5}$ in 2018 was 11.8 μg/m^3 (SD: ± 6.3 μg/m^3). • UFPs could be attributed to local combustion sources.	Aug. to Oct. 2021 (Data with 29 sets of MALDA and 1 set of MOUDI)
		Apr. to May 2022 (Data with 34 sets of MALDA and 1 set of MOUDI)
		Oct. to Dec. 2021 (Data with 37 sets of MALDA and 1 set of MOUDI)
UTHealth (SPH)	• Medical area • Located in the center of the Texas Medical Center. • Weekly-averaged $PM_{2.5}$ concentrations ranged between 7.9 and 13.3 μg/m^3 in 2014. • Surrounded by hospitals, universities, and residential houses and apartments. The source of UFPs is the local traffic.	Aug. to Sep. 2022 (Data with 25 sets of MALDA and 1 set of MOUDI)

lower airways (Marcias et al., 2018). To fill this gap, this study attempted to apply a newly developed Mobile Aerosol Lung Deposition Apparatus (MALDA) which covers a complete set of human airway replicas to measure real-life UFP respiratory deposition fractions and used a commercially available Micro-Orifice Uniform Deposit Impactor (MOUDI) to collect and analyze the composition of transition metals in urban UFPs. In this way, the respiratory deposited mass of transition metals and the transition metal-associated health risks caused by exposure to UFPs can be correctly estimated for people living in urban communities such as in the Greater Houston Area.

2. Method

2.1. Sampling sites

To study health risks caused by transition metals via UFP exposure in the Greater Houston Area, three sampling sites around the Houston urban area were selected for the field measurement. Table 2 lists detailed descriptions of the sampling sites. Among the three sampling sites, Park Place Blvd. (PP) and Clinton Dr. (CD) two sites are currently being maintained by the Houston Health Department (HHD). The third sampling site was located in the Texas Medical Center (TMC) at UTHealth School Public Health (SPH). These three sampling sites represent different communities in the Greater Houston Area having dissimilar UFP sources and profiles. The UFP at site PP is mainly due to the vehicle exhausts from nearby highways. The UFP sources of the site CD are expected to be truck exhausts and emissions from the refinery industries and the ship channel. The UFP source at site SPH is from the vehicle exhausts on the street in the hospital area. These sampling sites were selected based on previous studies on the characterization of airborne particulate matter (Han et al., 2017). Two sampling seasons were carried out at each sampling site during a one-year research time covering both hot and cool seasons. The field measurements were conducted in sequence among these three sampling sites during weekdays under ideal weather conditions.

2.2. Mobile aerosol lung deposition apparatus (MALDA)

MALDA was designed to carry out aerosol respiratory deposition experiments in real-life settings outside the laboratory to acquire realistic aerosol respiratory deposition data. MALDA consists of two systems: a human airway system and an aerosol measurement system. These two systems are placed on a cart, making the experimental setup movable to facilitate aerosol respiratory deposition field measurements. Fig. 1 shows the schematic diagram and physical photos of MALDA. MALDA is operated by a portable sampling pump at a continuous 30 L/min inspiratory (inhalation) flow rate, which corresponds to human minute ventilation (inhalation + exhalation) of 15 L/min under light activities. The human airway system of MALDA contains a set of realistic human airway replicas from nasal, oral, throat, trachea, tracheobronchial (TB) tree down to the 11th airway generation (bifurcation), and a representative alveolar region. The human airway replicas were made by 3D printing using conductive polylactic acid (PLA), and the inner surfaces of the airway replicas were coated with a thin layer of silicone oil. The representative alveolar region was constructed by porous conductive foams. Detailed descriptions of the TB airways and the representative alveolar region can be found in our previous publications (Su et al., 2019, 2021). In this study, the nasal airway was set to be the primary inlet for UFPs to enter the human airway system with the oral airway blocked.

The aerosol measurement system of MALDA contains two units of nanoparticle sizer (NanoScan 3910, TSI Inc., Shoreview, MN, USA) to measure UFP size distributions (size-dependent number concentration). UFP measurements were taken through four sampling probes installed at the nasal inlet, head outlet, TB tree outlet, and alveoli outlet of the human airway system. NanoScan is capable of measuring particle size

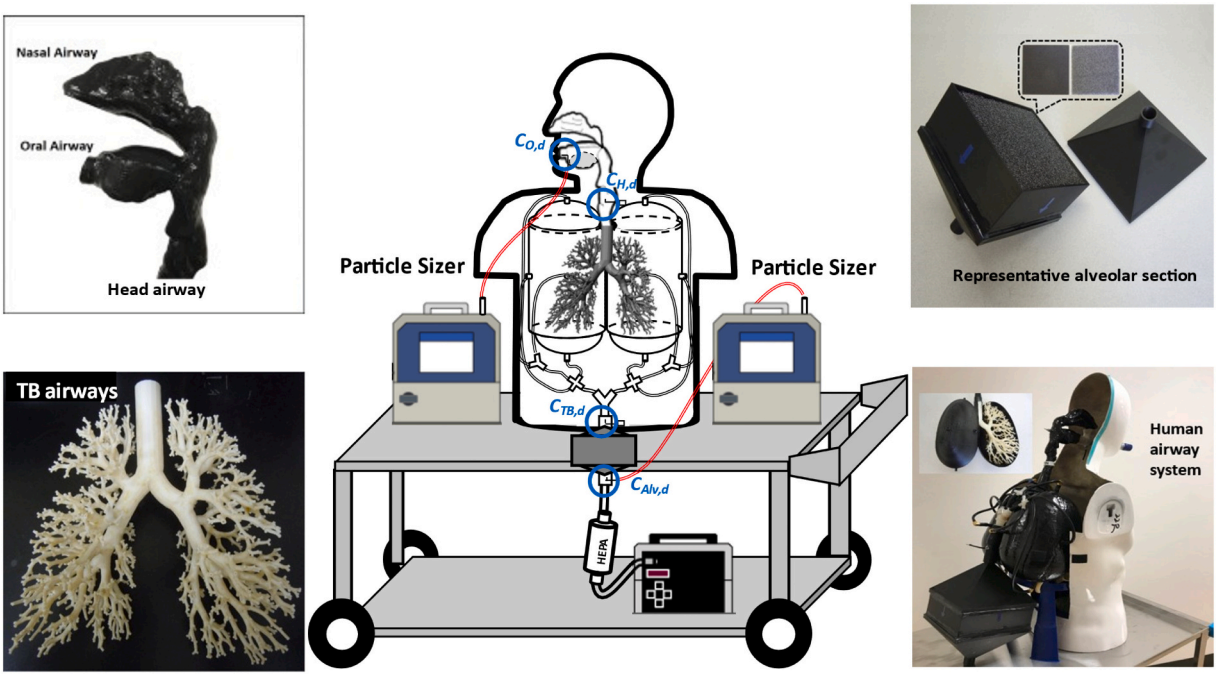

Fig. 1. The schematic and components of Mobile Aerosol Lung Deposition Apparatus (MALDA).

distributions of aerosol from 10 to 420 nm in a 1-min cycle with 13 size channels. UFPs <10 nm could not be measured due to the limitation of the instrument. The NanoScan was calibrated prior to the entire research, and the correction ratio between the two NanoScan units was recorded before each field measurement following the same experimental method employed previously (Su et al., 2019). By comparing the UFP size distribution measured at the nasal inlet to those at the major airway outlets, size-dependent UFP respiratory deposition in the head airways, TB tree, and alveolar region can be revealed. It has been proved that UFP respiratory deposition fractions obtained by MALDA agreed well with the conventional respiratory deposition curves published by the International Commission on Radiological Protection (ICRP) (ICRP, 1994; Hinds, 1999). In this study, whenever a field measurement was planned, MALDA was taken to the sampling locations to collect on-site UFP respiratory deposition information.

2.3. Micro-orifice uniform deposit impactor (MOUDI)

As mentioned previously, in order to correctly determine health risks induced by transition metals caused by urban UFP exposure, it is important to understand the composition of transition metals in urban UFPs. For this reason, a Micro Orifice Uniform Deposit Impactor (MOUDI 110 R, MSP Cooperation, Shoreview, MN) was employed to collect aerosol samples at the sampling sites. MOUDI is a commercially available multi-state aerosol cascade impactor that can collect aerosol particles with diameters from 56 nm to 18 μm on its 11 impactor stages. Each MOUDI impactor stage has a default collectible particle size range under the designed operation flow rate of 30 L/min. Particle samples collected on filters placed on each impactor stage can be used for gravimetric analysis and further used for chemical composition analyses to study aerosol composition. MOUDI has been used intensively in many ambient aerosol sampling research to collect size-segregated aerosol samples (Félix et al., 2015; Maudlin et al., 2015). In this study, MOUDI was deployed at the sampling sites during the whole sampling season to collect cumulative UFP samples for aerosol composition analysis.

2.4. Experimental procedure

During the sampling season of a sampling site, field measurements were scheduled based on weather conditions. MALDA was transported to the sampling site for field measurement only on days without rain. Three sampling timeframes were preselected for the MALDA field measurement: morning rush hours (9:00–10:00 a.m.), noon (12:00–1:00 p.m.), and afternoon rush hours (4:00–5:00 p.m.). The selection of these sampling timeframes attempted to cover potential high UFP concentration periods in a day to prevent underestimating the urban UFP exposure.

When operating MALDA, the nasal inlet of MALDA was always connected with one NanoScan to continuously measure the size distributions of UFPs entering the MALDA to record the temporal variations on the particle size distribution in the environment. The second set of NanoScan was used to measure the size distributions of UFPs at the head airways, TB tree, and alveolar region in sequence. For the measurement at each airway region, three particle size distributions were collected for calculating an average. In this way, UFP respiratory deposition fractions (*DF*) can be systematically estimated by the following equations:

$$DF_{Head,d} = \left(1 - \frac{C_{Head,d}}{C_{in,d}}\right), \quad (1)$$

$$DF_{TB,d} = \left(1 - \frac{C_{TB,d}}{C_{in,d}}\right) - \left(1 - \frac{C_{Head,d}}{C_{in,d}}\right), \quad (2)$$

$$DF_{Alv,d} = \left(1 - \frac{C_{Alv,d}}{C_{in,d}}\right) - \left(1 - \frac{C_{TB,d}}{C_{in,d}}\right), \quad (3)$$

where $DF_{Head,d}$, $DF_{TB,d}$, and $DF_{Alv,d}$ are size-dependent UFP respiratory deposition fractions (0 to 1.0) in the human head airways (*Head*), TB tree (*TB*), and the alveolar region (*Alv*), respectively. $C_{in,d}$ is the UFP size distribution measured at the MALDA nasal inlet. $C_{Head,d}$, $C_{TB,d}$, and $C_{Alv,d}$ are the UFP size distributions measured at the head outlet, TB outlet, and alveoli outlet, respectively. It is worth noting that C_{in} and C_{airway} were measured at the same time by the two NanoScan. Therefore, C_{airway}/C_{in} represents the penetration efficiency of UFP from the nasal inlet to a specific airway region in the human airway system. The 1- C_{airway}/C_{in}

represents the deposition fraction of UFP in a specific airway region. In this study, three runs (repeats) of MALDA respiratory deposition experiments were carried out in each field measurement for calculating the average. For each sampling timeframe of a sampling site, five to six field measurements were carried out during a sampling season.

On the other hand, MOUDI was placed at the sampling site throughout the whole sampling season for collecting daily UFP samples from 8:00 a.m. to 6:00 p.m. The reason for collecting UFP for such a long time was to accumulate a sufficient amount of UFP samples for consequent chemical analysis to investigate the composition of toxic transition metals present in urban UPFs. Before deploying MOUDI at the sampling site, pre-weighted 37 mm polytetrafluoroethylene (PTFE) membrane filters (PALL Co., Port Washington, NY, USA) were placed on each MOUDI impactor stage. When the sampling was completed, PTFE filters were unloaded from MOUDI and equilibrated in a temperature and humidity-controlled weighing room for one day. Then, filters were weighted individually using a high-accuracy microbalance (CAHN-34, ThermoFisher Scientific, Bedford, MA) to determine the total mass of aerosol collected on each MOUDI stage. After the gravimetric analysis, filters were processed, and transition metals were extracted by a modified US EPA IO-3.5 method (Mainey and William, 1999). Inductively coupled plasma-mass spectrometry system (ICP/MS) analysis was conducted to study the amount of transition metals (e.g., Fe, Zn, Cr, Cu, Mn, Ni, V, Co, Ag, and Cd) and other toxic and non-toxic metals (e.g., Al, Ba, Pb, Sb, Se, Sr, As, and U) present in the UFP samples. The metal analysis was implemented using an Agilent 7500ce ICP/MS (Agilent Technologies, Palo Alto, CA). Values below the limit of detection were assigned a value of two-thirds the value of the detection limit. Detailed descriptions of the metal extraction and analysis procedures can be seen in our previous study (Han et al., 2017). The results of the MOUDI analysis were the size-dependent metal-to-UFP mass ratio (*MR*). This information is essential for estimating the deposited mass of certain toxic transition metals in a person's airways resulting from urban UFP exposure.

2.5. Health risk estimation

Based on the UFP respiratory deposition fractions measured by MALDA, and the metal mass ratio found in UFPs by MOUDI, the hourly deposited mass (*DM*) of transition metals in major human airway regions can be estimated according to the following equations:

$$DM_{Head,k} = \sum_{d} \left[DF_{Head,d} \times MC_d \times MR_{k,d} \right] \times Q, \tag{4}$$

$$DM_{TB,k} = \sum_{d} \left[DF_{TB,d} \times MC_d \times MR_{k,d} \right] \times Q, \tag{5}$$

$$DM_{Alv,k} = \sum_{d} \left[DF_{Alv,d} \times MC_d \times MR_{k,d} \right] \times Q, \tag{6}$$

where $DM_{Head,k}$, $DM_{TB,k}$, and $DM_{Alv,k}$ are the hourly deposited mass (mg/h) of a specific transition metal, *k*, in the head airways (*Head*), TB tree (*TB*), and alveolar region (*Alv*), respectively. $DF_{Head,d}$, $DF_{TB,d}$, and $DF_{Alv,d}$ are size-dependent UFP respiratory deposition fractions (0 to 1.0) in head airways, TB tree, and the alveolar region (obtained by MALDA). MC_d is the size-dependent mass concentration of UFPs measured by NanoScan. The density of UFP used to calculate the mass of UFPs was assumed to be 1.5 g/cm^3 based on the published study (Slowik et al., 2004). $MR_{k,d}$ is the size-dependent mass ratio (mg/mg) of a transition metal, *k*, found in UFPs. *Q* is the total air volume inhaled by a person per hour, which is 0.9 (m^3/h) in this study for light outdoor activities.

Based on the *DM* calculated by Eqs. (4) to (6), the average daily dose, ADD_k (mg/kg-day), and the lifetime average daily dose, $LADD_k$ (mg/kg-day), of a specific transition metal (*k*) in a person's body resulting from urban UFP exposure can be calculated by:

$$ADD_k = \frac{\left(DM_{Head,k} + DM_{TB,k} + DM_{Alv,k}\right) \times (1 - LC) \times EH \times EF \times ED \times AB}{BW \times AT}, \tag{7}$$

$$LADD_k = \frac{\left(DM_{Head,k} + DM_{TB,k} + DM_{Alv,k}\right) \times (1 - LC) \times EH \times EF \times ED \times AB}{BW \times LT}, \tag{8}$$

where *LC* is the lung clearance ratio of the deposited substance (1- *LC* indicates the retention ratio of the respiratory deposited substance). *LC* was set to be 0 (0 %) in this study for worst-case scenario estimations. *EH* is the daily UFP exposure hours (hr/day) for a person living in the urban community. In this study, 3 h/day was used as a reasonable *EH* based on published statistics of outdoor exposure hours for a population living in areas with air pollution (Wu et al., 2010). *EF* is the exposure frequency (day/year), indicating the average days in a year a person is exposed to outdoor UFPs. *EF* is assumed to be 350 days/year based on the conventional exposure factor of US EPA (1989). *ED* is the exposure duration (year) which is the total years of a person's urban UFP exposure. In this study, the *ED* was set to be 30 years according to the conventional high-end exposure factor. *AB* is the absorption fraction of the deposited substance in the lung. In this study, *AB* was assumed to be 1.0 (100 %) for a conservative estimation. *BW* is the average human body weight and is 70 kg by default (US EPA, 1989). *AT* is the averaging time which is equal to the exposure duration (*ED*). *LT* is the default lifetime expectancy, which is 70 years (US EPA, 1989).

The calculated ADD_k was then used to estimate the non-cancer health risk by hazard quotient (*HQ*), which is the comparison of the ADD_k of a transition metal to the corresponding reference dose (*RfD*) of the transition metal:

$$HQ_k = ADD_k / RfD_k, \tag{9}$$

where RfD_k (mg/kg-day) is the reference dose published for a specific transition metal *k*. When the calculated HQ_k shows a value higher than 1.0, the non-cancer health effects induced by the transition metal, *k*, is considered potential (health risk is unacceptable). In addition, the hazard index (*HI*) was applied to all transition metals that induce the same non-cancer health effects. The *HI* is the summation of all related HQ_k (i.e. $HI = \sum HQ_k$). Similarly, when the calculated *HI* exceeds 1.0, the non-cancer effect caused by all related transition metals is considered potential. The overall non-cancer health risk is considered unacceptable.

The $LADD_k$ was used to estimate the lifetime excess cancer risk caused by the transition metal, *k*:

$$Cancer\ Risk = LADD_k \times CSF_k \tag{10}$$

where CSF_k (kg-day/mg) is the cancer slope factor of the transition metal, *k*. The cancer risk caused by transition metal, *k*, was considered unacceptable if the calculated lifetime excess cancer risk was higher than 1×10^{-6} (one in one million). In this study, published *RfD* and *CSF* for transition metals of concern were acquired from US EPA (IRIS), California EPA (CalEPA), and Agency for Toxic Substances and Disease Registry (ATSDR) websites and are all listed in Table 1.

In addition, since field measurements in this study were conducted for 17 months (May 2021- Sep. 2022) crossing different seasons, seasonal changes in UFP concentration and composition might affect the deposited mass as well as the associated health risks. Therefore, to correctly estimate health risks arising from UFP exposure throughout a year, it would be reasonable to combine data collected from different seasons (hot and cool) in the estimation of yearly UFP exposure. Houston is classified as subtropical climate, with approximately two-thirds of a year in the hot season (Mar. to Oct.) and one-third of the year in the cool season (Nov. to Feb.). Thus, respiratory deposition data and metal

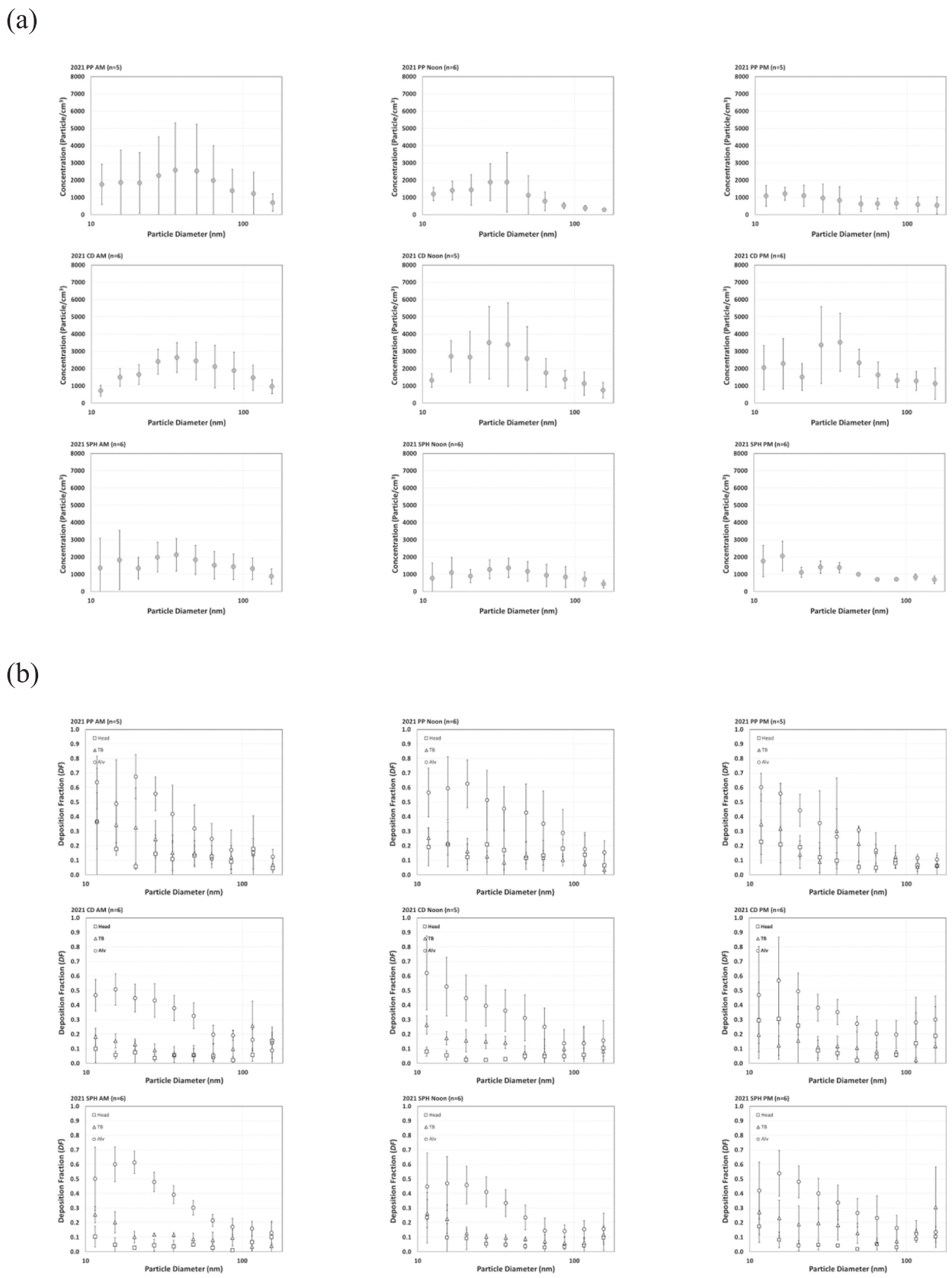

Fig. 2. UFP size distributions and respiratory depositions obtained by MALDA in 2021 from different sampling sites and sampling timeframes (a) particle size distributions, and (b) respiratory deposition (error bars represent the standard deviation of the measurement).

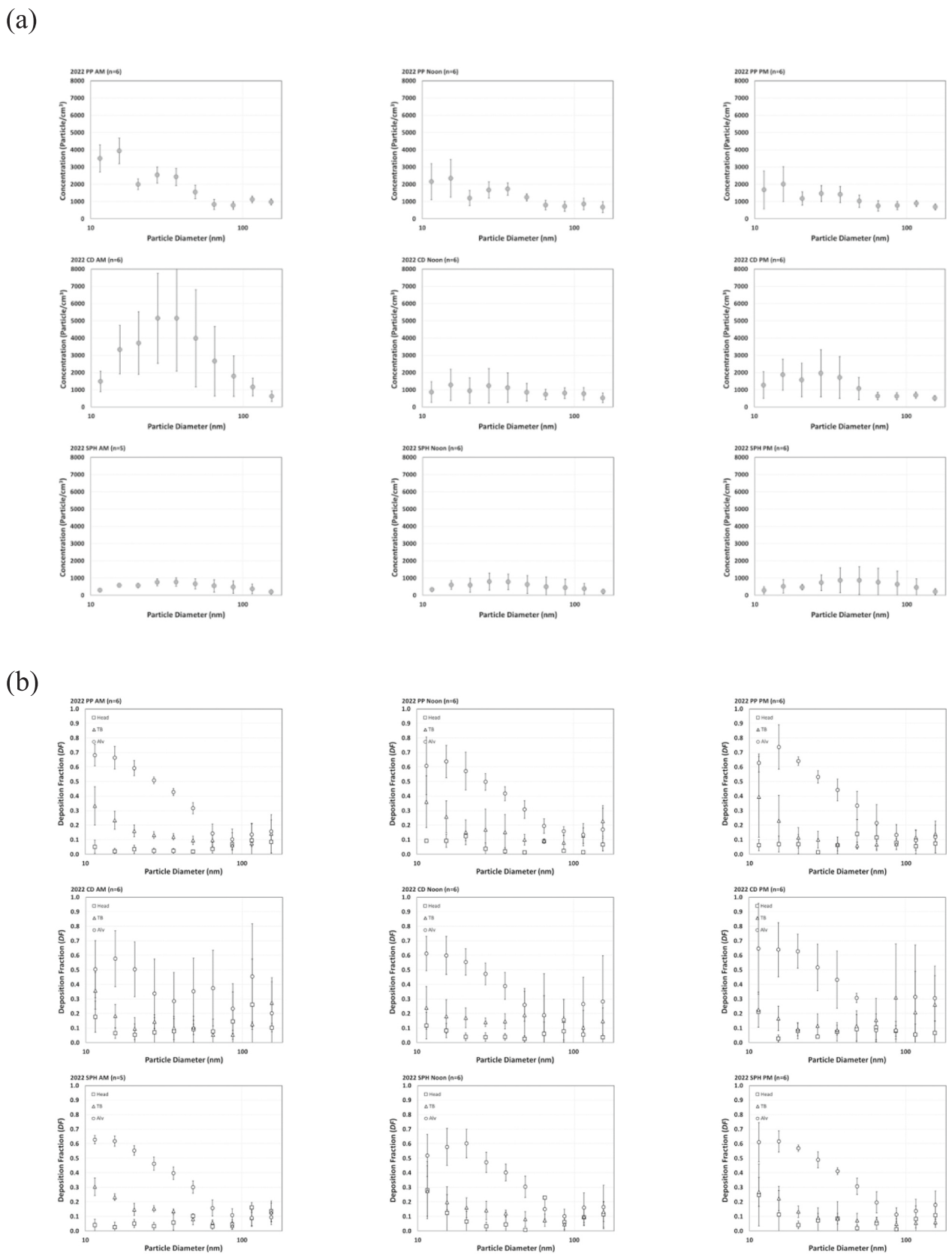

Fig. 3. UFP size distributions and respiratory depositions obtained by MALDA in 2022 from different sampling sites and sampling timeframes (a) particle size distributions, and (b) respiratory deposition (error bars represent the standard deviation of the measurement).

composition data acquired during the hot season accounted for the exposure condition from Mar. to Oct. in a year (two-thirds of a year), and data collected from the cool season accounted for the exposure condition from Nov. to Feb. in a year (one-third of a year). In this way, the non-cancer and cancer risks arising from exposure to transition metal-contained urban UFP can then be more correctly assessed for the population living in communities around the Greater Houston Area.

3. Results

3.1. UFP respiratory deposition fractions

Figs. 2(a) and 3(a) express the UFP size distributions (number concentration) measured during the field measurements in the years 2021 and 2022, individually. As can be seen, the size distributions of UFPs varied somewhat by sampling site, sampling timeframe, and sampling season. The sampling site CD shows a relatively higher particle number concentration than the other sites, and SPH generally shows the lowest. Most of the UFP size distributions presented a bell-shaped distribution with the peak shown at around the diameter of 40 nm. However, some of the measurements showed a bimodal size distribution, with another mode shown at around 15 nm. Data shown in Figs. 2(b) and 3(b) are the averaged size-dependent UFP respiratory deposition fractions in human head airways (*Head*), tracheobronchial tree (*TB*), and the alveolar region (*Alv*) obtained by MALDA at different sampling sites in different sampling timeframes (morning, noon, and afternoon). Fig. 2(b) shows the results obtained in the year 2021, and Fig. 3(b) shows the results in the year 2022. The size-dependent deposition fractions (*DF*) were calculated by Eqs. (1) to (3) for UFPs within the size range from 10 to 154 nm. It can be seen that UFP respiratory depositions exhibited similarities in deposition patterns unrelated to the sampling sites, sampling timeframes, and sampling seasons. Most inhaled UFPs were deposited in the alveolar region (*Alv*). Very few UFPs were deposited in the head airways (*Head*). High deposition fractions in the alveolar region were generated by UFPs from 15 to 20 nm. The corresponding deposition fractions were around 0.4 to 0.7. For UFPs larger than 20 nm, the deposition fraction decreased gradually with the increase in particle diameter. Low respiratory deposition fractions were found to be generated by particles larger than 100 nm.

3.2. UFP metal composition analysis

Fig. 4 (a) shows the size-dependent metal composition in aerosol from 56 to 320 nm based on target metals analyzed in this study. Aerosol samples were cumulative samples collected by MOUDI at three sampling sites during different sampling seasons. The metal composition is presented by the percentage of a specific metal among all metals analyzed in this study. Fig. 4(b) presents the metal-to-UFP mass ratio (mg/mg) for those toxic transition metals within specific size ranges. As mentioned previously, the mass of UFPs was obtained by gravimetric analysis, and the mass of transition metals contained in UFPs was acquired by ICP/MS analysis. It can be seen in Fig. 4 (b) that, for toxic metals, Cr had a relatively higher mass ratio in UFPs than the other transition metals, followed by Cu and Ba. No clear seasonal changes in the mass ratio were observed. The source of atmospheric Cr was reported to be emissions originating from traffic (fuel combustions) and industrial activities (Fernández et al., 2000). On the other hand, no representative or typical trend was found between the mass ratio and the particle diameter. For instance, the mass ratios of Cr, Cu, and Ba increased with the decrease in UFP diameter. However, for Mn, Ni, and Pb, their mass ratios in UFPs decreased with the increase in UFP diameter. Overall, except for Cr, most of the mass ratios of transition metals in UFPs were <0.001 in general.

3.3. Health risk estimation

Tables 3 and 4 list the estimated health risks induced by transition metals via exposure to the UFPs around the sampling sites. Risks were estimated by using Eqs. (7) to (10) according to the size-dependent UFP respiratory deposition data measured by MALDA from 10 to 115 nm shown in Figs. 2(b) and 3(b), and the size-dependent metal composition data obtained by MOUDI metal analysis in Fig. 4(b). It is worth noting that only toxic transition metals that have the potential to cause non-cancer or cancer health effects were used in the health risk estimation. Among these toxic transition metals, the mass of Cr found in UFPs represented the total chromium. Based on the published literature, the proportion of Cr (VI) in the total chromium was approximately 20–30 % in urban environments (Borai et al., 2002; Torkmahalleh et al., 2013). Therefore, 25 % was used as the proportion of Cr (VI) in the total chromium obtained in this study to calculate the mass of Cr (VI) for associated health risk estimations. The outdoor UFP exposure was based on daily outdoor activities of 3 h, with 1 h in the morning, noon, and afternoon, respectively. Health risks shown in Table 3 are initial health risks without considering UFP seasonal change. These health risks were estimated by using the MALDA and MOUDI data obtained from a certain sampling season as the representative exposure condition for the whole year for 30 years of exposure duration. Table 4 lists the health risks induced by transition metals calculated by taking into account the allocation of data collected from different seasons as described in the method section. The inclusion of seasonal variations in UFP concentration, respiratory deposition, and metal composition can more correctly present the health risks induced by transition metals caused by year-round urban UFP exposure. As shown in Tables 3 and 4, the transition metal-induced non-cancer risks arising from exposure to urban UFPs were generally acceptable around the Greater Houston Area. Calculated hazard quotients (HQ_k) and hazard index (*HI*) for all sampling sites were several orders <1.0, indicating non-cancer respiratory effects are not potential. On the other hand, transition metal-induced cancer risks estimated for people living in the Greater Houston Area near the sampling sites were also shown to be acceptable (risk $<10^{-6}$). The lung cancer risk caused by Cr (VI) showed a relatively higher risk than all the other transition metal-induced cancer risks. The calculated lifetime excess cancer risks were in order Cr (VI) $>$ As $>$ Ni $>$ Cd $>$ Pb. The highest lifetime excess cancer risks estimated was found at sampling site PP (2.7×10^{-7}) caused by Cr (VI), which is still within the conventional acceptable cancer risk.

4. Discussions

It is worth noting that the transition metal-associated daily doses and health risks estimated in this study are conservative or overestimated since they were calculated without considering the lung clearance and the epithelium absorption ratios in the respiratory system (lung clearance = 0; epithelium absorption = 1.0). It is known that airway self-clearing mechanisms can remove deposited objects from the human respiratory tract to prevent epithelium absorption or body uptake. By considering an airway self-clearing efficiency higher than 0 % and an epithelium absorption portion <100 %, the transition metal-associated daily doses and health risks can be further reduced. Thus, although the deposited mass of transition metals calculated in this study is regarded as bioavailable for respiratory absorption, the actual uptake amount becoming the daily dose should be much less. However, the health risks induced by transition metals through urban UFP exposure estimated in this study may serve as a purposely overestimated worst-case reference.

While this study focused on UFPs, it is known that ambient submicron aerosol with diameters larger than 100 nm possesses greater mass than UFPs. When these submicron particles deposit in the airways, they might result in a more deposited mass of transition metals in the human airways, leading to higher health risks. However, the size-dependent

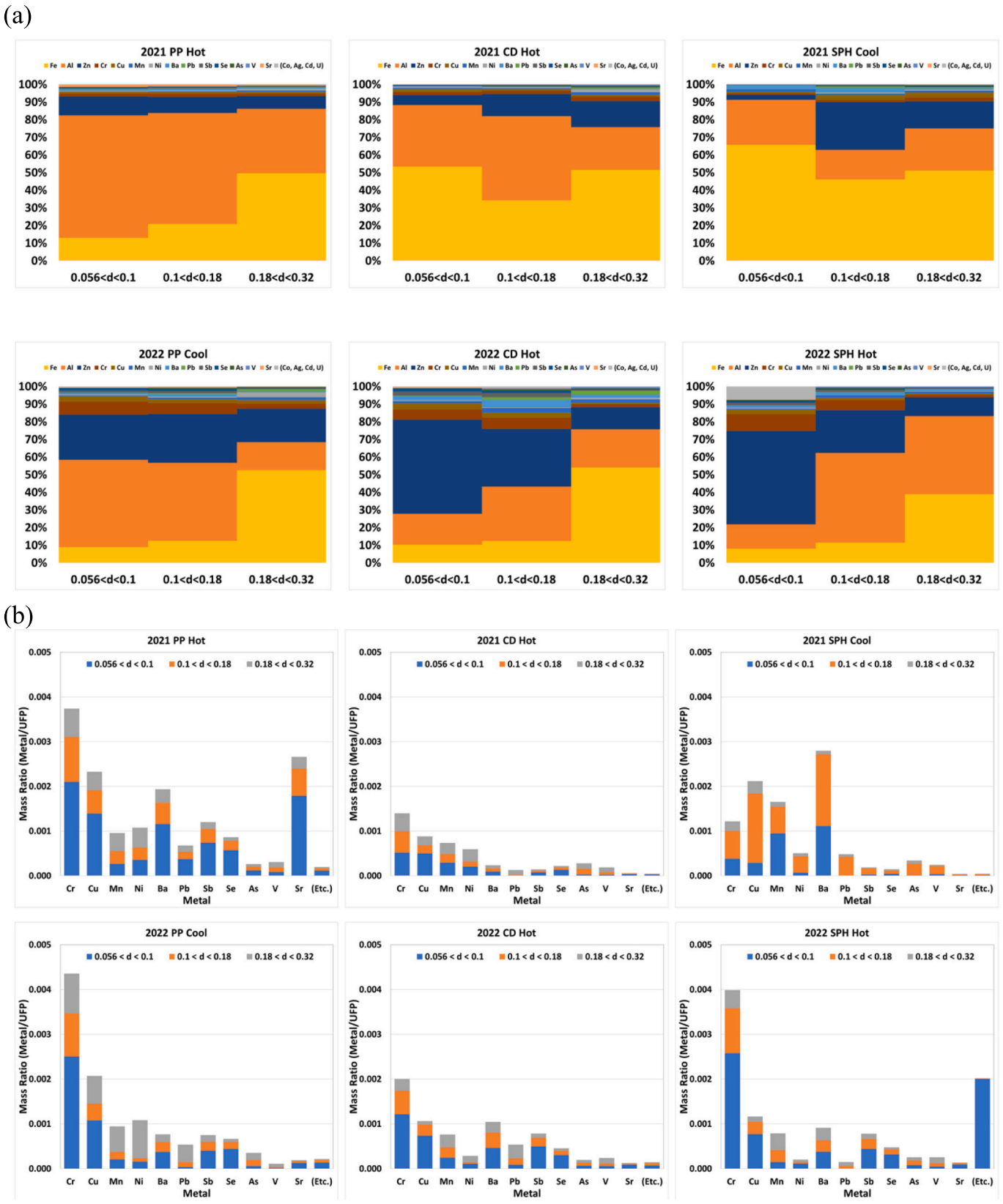

Fig. 4. MOUDI metal analysis for UFPs collected from different sampling locations and seasons (a) size-dependent metal composition for all metal analyzed ($n = 1$), and (b) metal-to-UFP mass ratios for toxic metals (n = 1).

Table 3
Estimated health risks arising from exposure to transition metals present in ambient UFP for communities around the Greater Houston Area.

No-cancer Risk											
Site	Cr	Mn	Pb	Ni	Sb	V	As	Co	Cd	U	HI[$]
2021 PP	5.0E-04	9.4E-04	–	6.0E-04	2.2E-04	1.5E-04	–	4.3E-05	5.3E-04	1.3E-07	3.0E-03
2021 CD	3.6E-04	1.6E-03	–	7.8E-04	4.6E-05	2.4E-04	–	2.3E-05	1.2E-04	1.5E-08	3.2E-03
2021 SPH	1.6E-04	1.5E-03	–	2.8E-04	3.0E-05	1.2E-04	–	1.3E-05	4.9E-05	6.3E-09	2.1E-03
2022 PP	5.9E-04	1.6E-03	–	1.2E-03	1.4E-04	9.4E-05	–	3.4E-06	1.0E-03	2.5E-08	4.6E-03
2022 CD	4.1E-04	1.4E-03	–	3.0E-04	2.1E-04	2.3E-04	–	3.9E-06	1.2E-03	2.9E-08	3.8E-03
2022 SPH	2.1E-04	3.8E-04	–	4.9E-05	5.5E-05	6.2E-05	–	1.1E-06	3.9E-03	1.3E-08	4.7E-03

Cancer Risk										
Site	Cr	Mn	Pb	Ni	Sb	V	As	Co	Cd	U
2021 PP	2.6E-07	–	1.8E-10	5.5E-09	–	–	2.5E-08	–	4.1E-09	–
2021 CD	1.9E-07	–	9.9E-11	7.2E-09	–	–	6.2E-08	–	9.2E-10	–
2021 SPH	8.0E-08	–	1.2E-10	2.6E-09	–	–	3.4E-08	–	3.8E-10	–
2022 PP	3.0E-07	–	2.6E-10	1.1E-08	–	–	4.8E-08	–	7.8E-09	–
2022 CD	2.1E-07	–	2.8E-10	2.8E-09	–	–	3.3E-08	–	9.0E-09	–
2022 SPH	1.1E-07	–	2.0E-11	4.5E-10	–	–	1.1E-08	–	3.0E-08	–

[$] Hazard Index (HI) is the summation of HQs of Cr, Mn, Ni, Sb, V, Co and Cd.

Table 4
Estimated health risks arising from exposure to transition metals present in ambient UFP for communities around the Greater Houston Area with considering hot and cool seasons.

No-cancer Risk											
Site	Cr	Mn	Pb	Ni	Sb	V	As	Co	Cd	U	HI[$]
PP	5.3E-04	1.2E-03	–	7.9E-04	1.9E-04	1.3E-04	–	3.0E-05	6.9E-04	9.2E-08	3.5E-03
CD[*]	3.9E-04	1.5E-03	–	5.4E-04	1.3E-04	2.4E-04	–	1.4E-05	6.4E-04	2.2E-08	3.5E-03
SPH	1.9E-04	7.5E-04	–	1.3E-04	4.7E-05	8.1E-05	–	5.0E-06	2.6E-03	1.1E-08	3.8E-03

Cancer Risk										
Site	Cr	Mn	Pb	Ni	Sb	V	As	Co	Cd	U
PP	2.7E-07	–	2.1E-10	7.3E-09	–	–	3.3E-08	–	5.3E-09	–
CD[*]	2.0E-07	–	1.9E-10	5.0E-09	–	–	4.7E-08	–	5.0E-09	–
SPH	9.7E-08	–	5.4E-11	1.2E-09	–	–	1.8E-08	–	2.0E-08	–

[$] Hazard Index (HI) is the summation of HQs of Cr, Mn, Ni, Sb, V, Co and Cd.
[*] Only hot season data were available.

respiratory deposition fraction of these submicron particles is known to be lower than that of UFPs. Furthermore, it was found during the field measurements that particle size distributions detected by NanoScan often showed sizes of up to 154 nm. Particles larger than 154 nm around 205, 273, and 365 nm were usually too low to be detected by NanoScan, indicating there seemed not much aerosol within the spectrum from 100 to 400 nm in the urban ambient air. As a result, the contribution of submicron particles to the health risk is uncertain with the competition between the more particle mass and the less particle deposition fraction and fewer particle concentration. Future studies are needed by using MALDA with particle sizers suitable for measuring submicron- or even micron-sized particles to comprehensively investigate health risks arising from exposure to the hazardous urban aerosol.

The MOUDI version employed in this study to collect UFP samples was model 110R with 11 impactor stages to collect aerosol from 56 nm to 18 μm. However, only data collected in the last three stages (56 to 320 nm) could be used in estimating health risks since they fall within the size range measured by NanoScan. Therefore, one limitation of this study was that the metal composition data obtained from the three MOUDI stages (56, 100, and 180 nm) were shared unevenly with 10 particle sizes from 10 to 154 nm measured by NanoScan for calculating the deposited mass and health risks. This allocation of the UFP composition data is considered not ideal and might introduce uncertainties to the final result. In the future, new versions of MOUDI should be used in UFP-related studies to acquire more detailed UFP composition data. For example, the newer MOUDI version, NanoMOUDI (122R or 125R), has seven of the 13 impactor stages designed to collect airborne particles from 10 to 320 nm. By using this device to sample UFPs, finer size-dependent UFP composition data could be acquired. Nevertheless, data obtained from this study using MOUDI 110R still showed valuable reference information to assess health risks induced by transition metals arising from urban UFP exposure.

Overall, from the viewpoint of health risk estimation caused by urban UFP exposure, the final health risk is determined by the concentration and composition of UFPs. Higher UFP concentration in the urban environment could lead to more respiratory deposited mass. An increased mass ratio of a toxic substance in UFPs would result in elevated daily doses and then health risks. Although the estimated health risks were found to be generally acceptable in this study, the health risk estimation was limited to transition metal-induced respiratory effects. It is known that respiratory effects and health problems can also be induced by other toxic substances contained in UFPs such as PAHs and BC. Indoor UFP exposure through daily activities such as cooking, candle burning, wood burning, and secondhand e-cigarette aerosol exposure can also contribute to overall UFP-induced health risks for certain populations. Therefore, in the future, when more size-dependent UFP chemical composition and respiratory deposition data are available and when more indoor UFP exposure studies are

conducted, a more comprehensive health risk assessment covering key UFP toxic substances and exposure scenarios can then be achieved. Finally, the health risk estimation in this study was based on healthy adults. Attention should be paid to sensitive urban populations (at-risk populations), including children, older adults, and people with certain pre-existing heart or lung diseases. Restricting outdoor UFP exposure hours for these sensitive populations or recommending wearing masks with high protection efficiencies during outdoor activities may be effective measures to mitigate the inhalation of urban UFPs and reduce health risks associated with transition metals. Data and findings acquired from this study can also be used as a reference for cities in the world having similar characteristics as Houston (port city, large population, heavy traffic, and oil refinery industry), such as Rotterdam (Netherlands), Tianjin (China), Mumbai (India), and Ulsan (Korea).

5. Conclusion

The utilization of MALDA and MOUDI proved to be effective experimental tools for acquiring on-site UFP respiratory deposition data and UFP composition data that are essential to assess health risks caused by UFP exposure. The experimental approach used in this study can be applied to other outdoor and indoor UFP exposure studies to estimate related deposited mass, daily dose, and health risks resulting from toxic substances present within UFPs. In this study, the estimated respiratory health risks induced by transition metals were within acceptable limits for urban UFP exposure around the Greater Houston Area. The transition metal-induced non-cancer risks indicated by hazard quotients and hazard indices were all below the threshold of 1.0. The transition metal-induced lifetime excess cancer risks were also found to be acceptable, with risk levels generally less than one in one million (10^{-6}).

CRediT authorship contribution statement

Conceptualization, W.S. and I.H.; methodology, W.S. and I.H.; validation, K.Z.; investigation, J.L. and M.A.; writing—original draft preparation, W.S., I.H. and K.Z.; funding acquisition, W.S. and I.H. All authors have read and agreed to the published version of the manuscript. The authors extend their gratitude to Beltz Patricia in the Houston Health Department (HHD) for facilitating access to the sampling sites to make the field measurement possible.

Declaration of competing interest

The authors declare that they have no known competing financial interests or personal relationships that could have appeared to influence the work reported in this paper.

Data availability

Data will be made available on request.

Acknowledgment

This research was funded by Grant Nos. R21ES031795 from the National Institute of Environmental Health Sciences (NIEHS), 19TPA34830085 from the American Heart Association, and 5T42OH008421 from the National Institute for Occupational Safety and Health (NIOSH) to the Southwest Center for Occupational and Environmental Health (SWCOEH).

References

Bahreini, R., Ervens, B., Middlebrook, A.M., Warneke, C., De Gouw, J.A., DeCarlo, P.F., Jimenez, J.L., Brock, C.A., Neuman, J.A., Ryerson, T.B., Stark, H., 2009. Organic aerosol formation in urban and industrial plumes near Houston and Dallas, Texas. J. Geophys. Res.-Atmos. 114 (D7) https://doi.org/10.1029/2008JD011493.

Bhatia, R., Lopipero, P., Smith, A.H., 1998. Diesel exhaust exposure and lung cancer. Epidemiology 9 (1), 84–91.

Borai, E.H., El-Sofany, E.A., Abdel-Halim, A.S., Soliman, A.A., 2002. Speciation of hexavalent chromium in atmospheric particulate samples by selective extraction and ion chromatographic determination. TRAC-Trend. Anal. Chem. 21 (11), 741–745. https://doi.org/10.1016/S0165-9936(02)01102-0.

Carter, J.D., Ghio, A.J., Samet, J.M., Devlin, R.B., 1997. Cytokine production by human airway epithelial cells after exposure to an air pollution particle is metal-dependent. Toxicol. Appl. Pharm. 146 (2), 180–188. https://doi.org/10.1006/taap.1997.8254.

Chen, L.C., Lam, H.F., Kim, E.J., Guty, J., Amdur, M.O., 1990. Pulmonary effects of ultrafine coal fly ash inhaled by guinea pigs. J. Toxicol. Env. Heal. A. 29 (2), 169–184. https://doi.org/10.1080/15287399009531381.

Chen, Y., Shah, N., Huggins, F.E., Huffman, G.P., Dozier, A., 2005. Characterization of ultrafine coal fly ash particles by energy-filtered TEM. J. Microsc-Oxford 217 (3), 225–234. https://doi.org/10.1111/j.1365-2818.2005.01445.x.

Cheng, Y.S., Su, Y.F., Yeh, H.C., Swift, D.L., 1993. Deposition of thoron progeny in human head airways. Aerosol Sci. Tech. 18 (4), 359–375. https://doi.org/10.1080/02786829308959610.

Cohen, B.S., Sussman, R.G., Lippmann, M., 1990. Ultrafine particle deposition in a human tracheobronchial cast. Aerosol Sci. Tech. 12 (4), 1082–1091. https://doi.org/10.1080/02786829008959418.

Donaldson, K., Stone, V., Gilmour, P.S., Brown, D.M., MacNee, W., 2000. Ultrafine particles: mechanisms of lung injury. Philos. T. Roy. Soc. A. 358 (1775), 2741–2749. https://doi.org/10.1098/rsta.2000.0681.

Donaldson, K., Stone, V., Seaton, A., MacNee, W., 2001. Ambient particle inhalation and the cardiovascular system: potential mechanisms. Environ. Health Persp. 109 (Suppl. 4), 523–527. https://doi.org/10.1289/ehp.01109s4523.

Félix, O.I., Csavina, J., Field, J., Rine, K.P., Sáez, A.E., Betterton, E.A., 2015. Use of lead isotopes to identify sources of metal and metalloid contaminants in atmospheric aerosol from mining operations. Chemosphere 122, 219–226. https://doi.org/10.1007/s11270-011-0777-x.

Fernández, A.J., Ternero, M., Barragán, F.J., Jiménez, J.C., 2000. An approach to characterization of sources of urban airborne particles through heavy metal speciation. Chemosphere 2 (2), 123–136. https://doi.org/10.1016/S1465-9972(00)00002-7.

Gangwar, C., Choudhari, R., Chauhan, A., Kumar, A., Singh, A., Tripathi, A., 2019. Assessment of air pollution caused by illegal e-waste burning to evaluate the human health risk. Environ. Int. 125, 191–199. https://doi.org/10.1016/j.envint.2018.11.051.

Han, I., Guo, Y., Afshar, M., Stock, T.H., Symanski, E., 2017. Comparison of trace elements in size-fractionated particles in two communities with contrasting socioeconomic status in Houston, TX. Environ. Monit. Assess. 189, 1–13. https://doi.org/10.1007/s10661-017-5780-2.

Hinds, W.C., 1999. Aerosol Technology: Properties, Behavior, and Measurement of Airborne Particles. John Wiley & Sons.

Ibald-Mulli, A., Wichmann, H.E., Kreyling, W., Peters, A., 2002. Epidemiological evidence on health effects of ultrafine particles. J. Aerosol Med. 15 (2), 189–201. https://doi.org/10.1089/089426802320282310.

ICRP, 1994. Human respiratory tract model for radiological protection. ICRP publication 66. Ann. ICRP 24, 1–3.

Langrish, J.P., Unosson, J., Bosson, J., Barath, S., Muala, A., Blackwell, S., Söderberg, S., Pourazar, J., Megson, I.L., Treweeke, A., Sandström, T., 2013. Altered nitric oxide bioavailability contributes to diesel exhaust inhalation-induced cardiovascular dysfunction in man. J. Am. Heart Assoc. 2 (1), e004309 https://doi.org/10.1161/JAHA.112.004309.

Mainey, A., William, T., 1999. Compendium of Methods for the Determination of Inorganic Compounds in Ambient Air:(Chapter IO-3) Chemical Species Analysis of Filter-Collected Suspended Particulate Matter. US Environmental Protection Agency.

Marcias, G., Fostinelli, J., Catalani, S., Uras, M., Sanna, A.M., Avataneo, G., De Palma, G., Fabbri, D., Paganelli, M., Lecca, L.I., Buonanno, G., 2018. Composition of metallic elements and size distribution of fine and ultrafine particles in a steelmaking factory. Int. J. Environ. Res. Pu. 15 (6), 1192. https://doi.org/10.3390/ijerph15061192.

Maudlin, L.C., Wang, Z., Jonsson, H.H., Sorooshian, A., 2015. Impact of wildfires on size-resolved aerosol composition at a coastal California site. Atmos. Environ. 119, 59–68. https://doi.org/10.1016/j.atmosenv.2015.08.039.

Micic, M., Leblanc, R.M., Markovic, D., Stamatovic, A., Vukelic, N., Polic, P., 2003. Atlas of the tropospheric aerosols from Belgrade troposphere. Fresen. Environ. Bull. 12 (9), 1015–1024.

Moreno-Rıos, A.L., Tejeda-Benıtez, L.P., Bustillo-Lecompte, C.F., 2022. Sources, characteristics, toxicity, and control of ultrafine particles: an overview. Geosci. Front. 13 (1), 101147 https://doi.org/10.1016/j.gsf.2021.101147.

Oberdörster, G., Sharp, Z., Atudorei, V., Elder, A., Gelein, R., Kreyling, W., Cox, C., 2004. Translocation of inhaled ultrafine particles to the brain. Inhal. Toxicol. 16 (6–7), 437–445. https://doi.org/10.1080/08958370490439597.

Ohlwein, S., Kappeler, R., Kutlar Joss, M., Künzli, N., Hoffmann, B., 2019. Health effects of ultrafine particles: a systematic literature review update of epidemiological evidence. Int. J. Public Health 64, 547–559. https://doi.org/10.1007/s00038-019-01202-7.

Schraufnagel, D.E., 2020. The health effects of ultrafine particles. Exp. Mol. Med. 52 (3), 311–317. https://doi.org/10.1038/s12276-020-0403-3.

Shang, Y., Chen, R., Bai, R., Tu, J., Tian, L., 2021. Quantification of long-term accumulation of inhaled ultrafine particles via human olfactory-brain pathway due to environmental emissions–a pilot study. NanoImpact 22, 100322. https://doi.org/10.1016/j.impact.2021.100322.

Slowik, J.G., Stainken, K., Davidovits, P., Williams, L.R., Jayne, J.T., Kolb, C.E., Worsnop, D.R., Rudich, Y., DeCarlo, P.F., Jimenez, J.L., 2004. Particle morphology

and density characterization by combined mobility and aerodynamic diameter measurements. Part 2: application to combustion-generated soot aerosols as a function of fuel equivalence ratio. Aerosol Sci. Tech. 38 (12), 1206–1222. https://doi.org/10.1080/027868290903916.

Smith, S., Cheng, Y.S., Yeh, H.C., 2001. Deposition of ultrafine particles in human tracheobronchial airways of adults and children. Aerosol Sci. Tech. 35 (3), 697–709. https://doi.org/10.1080/02786820152546743.

Sørensen, M., Schins, R.P., Hertel, O., Loft, S., 2005. Transition metals in personal samples of PM2. 5 and oxidative stress in human volunteers. Cancer Epidem. Biomar. 14 (5), 1340–1343. https://doi.org/10.1158/1055-9965.EPI-04-0899.

Su, W.C., Cheng, Y.S., 2015. Estimation of carbon nanotubes deposition in a human respiratory tract replica. J. Aerosol Sci. 79, 72–85. https://doi.org/10.1016/j.jaerosci.2014.09.005.

Su, W.C., Chen, Y., Xi, J., 2019. A new approach to estimate ultrafine particle respiratory deposition. Inhal. Toxicol. 31 (1), 35–43. https://doi.org/10.1080/08958378.2019.1576808.

Su, W.C., Wong, S.W., Buu, A., 2021. Deposition of E-cigarette aerosol in human airways through passive vaping. Indoor Air 31 (2), 348–356. https://doi.org/10.1111/ina.12754.

Torkmahalleh, M.A., Yu, C.H., Lin, L., Fan, Z., Swift, J.L., Bonanno, L., Rasmussen, D.H., Holsen, T.M., Hopke, P.K., 2013. Improved atmospheric sampling of hexavalent chromium. J. Air Waste Manage. Assoc. 63 (11), 1313–1323. https://doi.org/10.1080/10962247.2013.823894.

United States. Environmental Protection Agency, Office of Health and Environmental Assessment. Exposure Assessment Group, 1989. Exposure factors handbook (Vol. 90, no. 106774). Office of Health and Environmental Assessment, US Environmental Protection Agency.

Utsunomiya, S., Jensen, K.A., Keeler, G.J., Ewing, R.C., 2004. Direct identification of trace metals in fine and ultrafine particles in the Detroit urban atmosphere. Environ. Sci. Technol. 38 (8), 2289–2297. https://doi.org/10.1021/es035010p.

Wei, Y., Han, I.K., Shao, M., Hu, M., Zhang, J., Tang, X., 2009. PM2. 5 constituents and oxidative DNA damage in humans. Environ. Sci. Technol. 43 (13), 4757–4762. https://doi.org/10.1021/es803337c.

Wierzbicka, A., Nilsson, P.T., Rissler, J., Sallsten, G., Xu, Y., Pagels, J.H., Albin, M., Österberg, K., Strandberg, B., Eriksson, A., Bohgard, M., 2014. Detailed diesel exhaust characteristics including particle surface area and lung deposited dose for better understanding of health effects in human chamber exposure studies. Atmos. Environ. 86, 212–219. https://doi.org/10.1016/j.atmosenv.2013.11.025.

Wittkopp, S., Staimer, N., Tjoa, T., Gillen, D., Daher, N., Shafer, M., Schauer, J.J., Sioutas, C., Delfino, R.J., 2013. Mitochondrial genetic background modifies the relationship between traffic-related air pollution exposure and systemic biomarkers of inflammation. PloS One 8 (5), e64444. https://doi.org/10.1371/journal.pone.0064444.

Wu, X.M., Fan, Z.T., Ohman-Strickland, P., 2010. Time-location patterns of a population living in an air pollution hotspot. J. Environ. Public Health 2010. https://doi.org/10.1155/2010/625461.